# Merged-beam measurements of absolute cross sections for electron-impact excitation of $S^{4+}$ ($3s^2\ ^1S \rightarrow 3s3p\ ^1P$) and $S^{5+}$ ($3s\ ^2S \rightarrow 3p\ ^2P$)

B. Wallbank
*Department of Physics, St. Francis Xavier University, Antigonish, Nova Scotia, Canada B2G 2W5*

M. E. Bannister* and H. F. Krause
*Physics Division, Oak Ridge National Laboratory, Oak Ridge, Tennessee 37831-6372, USA*

Y.-S. Chung
*Department of Physics, Chungnam National University, 305-764, Daejon, Korea*

A. C. H. Smith
*Department of Physics and Astronomy, University College London, London WC1E 6BT, United Kingdom*

N. Djurić† and G. H. Dunn
*JILA, University of Colorado and National Institute of Standards and Technology, Boulder, Colorado 80309-0440, USA*
(Received 3 January 2007; published 3 May 2007)

Absolute cross sections for electron-impact excitation of the dipole-allowed transitions $S^{4+}$ ($3s^2\ ^1S \rightarrow 3s3p\ ^1$P) and $S^{5+}$ ($3s\ ^2S \rightarrow 3p\ ^2P$) were measured near threshold using the merged electron-ion beams energy-loss technique. Although the magnitudes of the measured cross sections are in reasonable agreement with available theoretical data, the experimental data indicate that the contributions of dielectronic resonances in the near-threshold region are underestimated by these calculations.

DOI: 10.1103/PhysRevA.75.052703 PACS number(s): 34.80.Kw

## I. INTRODUCTION

Since the dynamics of plasmas are usually dominated by electrons and positive ions and their interactions, detailed information about these interactions is critical for modeling and diagnostics. Careful experimental benchmarks are necessary for verifying the predictions of theoretical calculations, which produce much of the electron-ion collision data required by plasma science. Of particular interest are interactions of electrons with Na-like ions because their line emissions are commonly used as spectroscopic diagnostics of plasma parameters such as electron temperature [1,2]. Transitions of Mg-like ions are also commonly observed in emission spectra from plasma environments [3,4]. Electron-impact excitation cross sections have been previously measured in our laboratory and at the Jet Propulsion Laboratory with the merged-beams energy-loss technique for some Na-like ions ($Mg^+$, $Al^{2+}$, $Si^{3+}$, $Cl^{6+}$, $Ar^{7+}$) [5–9] and Mg-like ions ($Si^{2+}$, $Cl^{5+}$, $Ar^{6+}$) [8,10,11] in the third row of the periodic table. In this paper, absolute excitation cross sections are reported for the first allowed transitions in Mg-like $S^{4+}$ and Na-like $S^{5+}$. These ions are found in astrophysical plasmas such as the Io torus [12] and the AG Draconis nebula [13]. Perhaps more importantly, the experimental data reported here will serve as benchmarks for refining theoretical techniques such as close-coupling *R*-matrix (CCR) and convergent close-coupling calculations which are relied upon for the production of most of the excitation data needed by the plasma science community.

Electron-impact excitation of multiply charged ions can occur through both direct excitation and the indirect process of resonant dielectronic capture into a doubly excited state followed by autoionization to an excited state. These processes are represented for the excitation of the first dipole-allowed transition in $S^{4+}$, for example, as

$$e(E_i) + S^{4+}(3s^2\ ^1\mathrm{S}) \rightarrow S^{4+}(3s3p^1\ P) + e(E_f) \qquad (1a)$$

$$e(E_i) + S^{4+}(3s^2\ ^1\mathrm{S}) \rightarrow S^{3+}(3snln'l') \rightarrow S^{4+}(3s3p^1\ P) + e(E_a), \qquad (1b)$$

where $E_i$, $E_f$, and $E_a$ are the electron initial, final, and Auger energies, respectively.

Interactions between the $nln'l'$ states of the recombined ion and interference between the direct and indirect processes are important, so measurements of these systems can provide a sensitive benchmark of close-coupling predictions that include these effects. Here we report measurements of absolute cross sections for electron-impact excitation of the first dipole-allowed transitions in $S^{4+}$ and $S^{5+}$ performed using the merged electron-ion beams energy-loss (MEIBEL) technique.

## II. EXPERIMENT

### A. Ion beams

Sulfur ions were extracted at a fixed potential of 18 kV from the ORNL Caprice electron-cyclotron-resonance (ECR) ion source [14] and magnetically mass-to-charge analyzed.

*Electronic address: bannisterme@ornl.gov
†Present address: Jet Propulsion Laboratory, 4800 Oak Grove Drive, Pasadena, CA 91109.

 

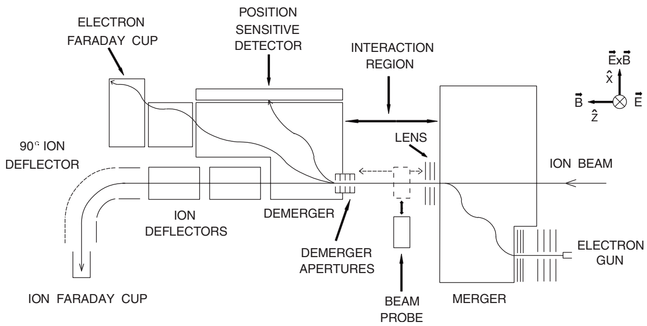


FIG. 1. Schematic of the JILA/ORNL MEIBEL apparatus. See text for details.

The ion source gas was carbon disulphide ($CS_2$) vapor produced in a reservoir warmed to a few degrees above room temperature by a water bath. The gas lines were also heated to prevent condensation between the reservoir and the ion source. The $CS_2$ reservoir was frozen with liquid nitrogen and then evacuated to remove all air from the reservoir before warming it. This was done to eliminate oxygen from the gas feed system since $^{16}O^{2+}$ could not be separated from $^{32}S^{4+}$ ions by the magnetic analysis. By comparing the $^{32}S:^{34}S$ isotope ratios for the +3, +4, and +5 charge states, we determined that the oxygen contamination in the $^{32}S^{4+}$ ion beams was less than 2% since the $^{32}S^{3+}$ and $^{32}S^{5+}$ ions beams are not contaminated with any oxygen ions of the same mass-to-charge ratio. The isotope ratio measurements were repeated periodically during the experiment to ensure that the contamination level did not change. As a trial of oxygen contamination effects, some measurements on $S^{4+}$ were made at the beginning of the experiment with up to 20% oxygen contamination; these data are considered relative and were normalized against the later measurements made with contamination less than 2%.

### B. MEIBEL apparatus

Details of the merged-beams apparatus and experimental method have been published previously [15], so only an overview will be presented here. A schematic diagram of the JILA/ORNL MEIBEL apparatus is shown in Fig. 1. Electrons produced by a gun featuring a dispenser-type cathode are merged with the $S^{q+}$ ions using a trochoidal analyzer. This "merger" employs crossed **E** and **B** fields to displace the electron beam by about 64 mm perpendicular to both fields. The electrons undergo two gyrations in the **B** field while traversing the merger, ensuring that the electron beam velocity in the interaction region remains parallel to that of the ion beam. After traversing an electric-field-free merge path (68.5 mm long) in the uniform solenoidal magnetic field (~4 mT), the electrons are separated from the ions by a second trochoidal analyzer. This "demerger" deflects electrons that are inelastically scattered from ions onto a position-sensitive detector (PSD) consisting of a pair of microchannel plates (MCPs) and a resistive anode. The primary (unscattered) electrons are deflected through a smaller angle where they are collected in a Faraday cup. The ions pass through the demerger with negligible deflection and are usually collected in another Faraday cup after being bent through 90°. For these investigations, however, an internal fault on this cup prevented its use for current measurements. Current measurements were performed immediately before and after each cross-section measurement, using a Faraday cup located upstream of the interaction region (not shown in Fig. 1). Electrons elastically scattered through large angles can also reach the PSD since their forward velocities are close to those of inelastically scattered electrons. However, this is prevented by a series of five apertures (6.5 mm diameter) located at the entrance of the demerger, because these elastically scattered electrons have much larger cyclotron radii in the **B** field than in the inelastically scattered electrons with the same forward velocity.

In addition to the signal from the inelastic scattering events, large background count rates from electron and ion scattering on residual gas and surfaces are present on the PSD. In order to extract the signal from these backgrounds, both beams are chopped in a phased four-way pattern [15] and counts from the detector are accumulated in four histogramming memories, preserving the position information. The detector counts in the four two-dimensional histograms are individually corrected for the dead times of the position computer, the histogram interface, and the microchannel plates. The inelastic signal as a function of position on the PSD is then obtained from appropriate addition and subtraction of the corrected counts in the four histograms.

### C. Cross-section determination

The excitation cross section $\sigma$ at an interaction energy in the center-of-mass system, $E_{c.m.}$, is determined from

$$\sigma(E_{c.m.}) = \frac{R}{\varepsilon}\left|\frac{v_e v_i}{v_e - v_i}\right|\frac{qe^2}{I_e I_i}F, \qquad (2)$$

where $R$ is the signal count rate of the inelastically scattered electrons, and $v_e$, $v_i$, $I_e$, and $I_i$ are the laboratory velocities and currents of the electrons and ions of charge magnitudes $e$ and $qe$, respectively. The absolute PSD detection efficiency $\varepsilon$ was measured to be $0.55 \pm 0.02$ by alternately directing a small beam of electrons, with a current of tens of femtoamperes, onto the PSD and into the electron Faraday cup to be measured by a calibrated vibrating reed electrometer. The form factor $F$ is given by

$$F = \frac{\int G(x,y,z)dx\,dy \int H(x,y,z)dx\,dy}{\int G(x,y,z)H(x,y,z)dx\,dy\,dz}. \qquad (3)$$

The densities of the two beams, $G(x,y,z)$ and $H(x,y,z)$, are measured with a movable video probe [16] at several positions along the interaction region. The probe consists of a microchannel plate backed by a phosphor-coated coherent fiber optic bundle to convert the incident particles into an optical signal that is then digitized by a charge-injection device (CID) camera chip [17]. The video signals from the CID camera are then recorded by a frame grabber card and stored on the probe control computer to facilitate the numerical integration of Eq. (3). A grounded grid (50% transmission) in front of the probe allows the electrons to be accelerated through an additional 75 V before striking the MCP.

The data-taking protocol consists of first tuning the electron and ion beams to obtain minimum backgrounds. A simultaneous effort is made to obtain a reasonably good overlap in the interaction region, but with no overlap within and after the demerger apertures in order to prevent elastically scattered electrons from reaching the PSD. This is accomplished by producing a well-collimated electron beam and then sloping the ion beam down through it. A form factor is then determined from the measured beam densities. The ion current is measured and integrated for 120 s in a Faraday cup located upstream of the interaction region. Data are collected at a given center-of-mass energy $E_{c.m.}$ until the required statistical precision is reached. The ion current measurements are then repeated. $E_{c.m.}$ is then changed a few percent to a new value by precisely scaling the magnetic field and the voltages on the electron gun, merger, and demerger before more data are taken at this new energy. This procedure is repeated several times to cover a given energy range. Beam profiles are measured again after data collection at several energies to check that the form factor has not deviated significantly during the scalings of the electron configuration.

### D. Adjustments to data

#### *1. Center-of-mass energy scale*

The absolute energy scale of the measurements was determined by fitting the experimental data for the $S^{4+}$ ($3s^2\ 1S \rightarrow 3s3p\ ^1P$) transition within 0.5 eV of the apparent threshold with a step function at the spectroscopic threshold of 15.76 eV that was convoluted with a Gaussian representing the experimental energy distribution. This fitting procedure yielded a cathode contact potential of 1.80 V and an energy spread full width at half maximum (FWHM) of 0.17 eV. The energy scale of all sets of excitation data were then corrected using this fitted cathode contact potential.

#### *2. Metastable ions*

Based on our previous measurements on Mg-like ions [8,10,11], we expected that a significant fraction of the $S^{4+}$ ions extracted from the ion source would be in $3s3p\ ^3P$ metastable states with a lifetime much longer than the 1 $\mu$s flight time to the MEIBEL apparatus. To determine the metastable fraction in the beam, electron-impact ionization cross sections for the mixed-state $S^{4+}$ ion beam were measured using the ORNL crossed-beam apparatus [18,19] from below the ionization threshold of the metastable state (62.3 eV) to 150 eV. The experimental ionization cross sections are shown as the plotted points in Fig. 2. The onset of ionization clearly occurs below the ionization threshold for the $3s^2\ ^1S$ ground-state ions (72.7 eV). Using the procedure detailed in previous investigations of Mg-like ions [8,10,11], we least-squares fitted the experimental data with a scaled Lotz formula [20], with the two fitting parameters being the ion beam metastable fraction and a scaling factor. The fit is shown as the solid curve in Fig. 2. The metastable fraction

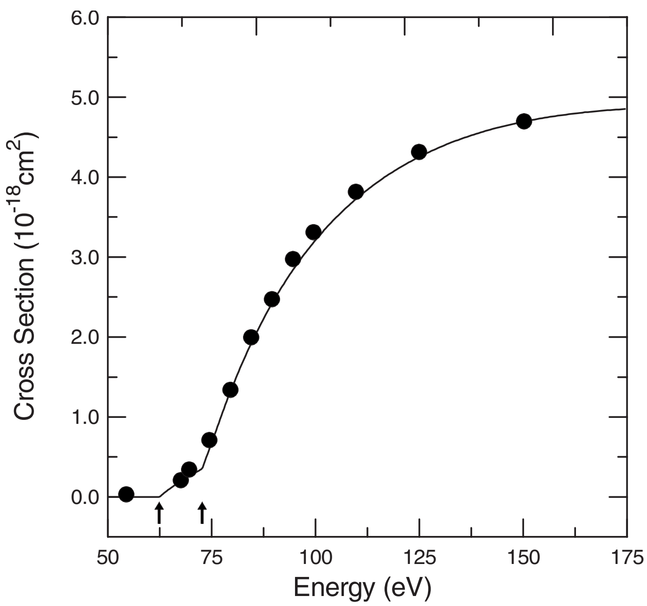


FIG. 2. Absolute cross sections for ionization of $S^{4+}$ by electron impact as a function of center-of-mass energy. Solid circles are present results; error bars representing a 90% confidence level of relative uncertainties are smaller than the circles. The solid curve is a least-squares fit of a scaled Lotz formula for the mixture of ground-state and metastable ions. The metastable fraction determined by this fit is $0.31 \pm 0.03$; see the text for an explanation. The arrows represent the thresholds for the $3s3p\ ^3P$ metastable and the $3s^2\ ^1S$ ground-state ions of 62.3 and 72.7 eV, respectively.

was determined to be $0.31 \pm 0.03$ with the uncertainty given at a one-standard-deviation level. The ion currents recorded in the measurements of the excitation of $S^{4+}$ were corrected for this since only ground-state ions contribute to the studied transition.

No metastable ions are expected in the Na-like $S^{5+}$ ion beam extracted from the ECR ion source since none were observed in previous ionization measurements of Na-like ions [21–23] produced under similar source conditions.

#### *3. Below-threshold spurious signal*

Despite extreme care in preventing elastically scattered electrons from reaching the PSD and in reducing the individual backgrounds of the two beams, a persistent in-phase signal was measured below the excitation thresholds. This signal was likely due to the modulation of the background of one beam by the space charge of the other beam. This apparent background cross section was found to be independent of the center-of-mass energy, and was constant in time; consequently, it was subtracted from all the measured cross sections. Additional uncertainty for this subtraction procedure was included in the total experimental uncertainty, as discussed below.

#### *4. Signal losses in the demerger*

At center-of-mass energies sufficiently above the excitation threshold, the scattered electron velocity can exceed the ion velocity, so that an electron scattered at a large enough

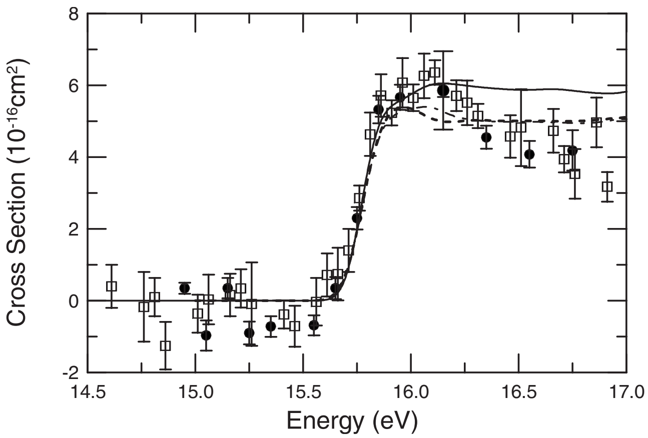


FIG. 3. Absolute cross sections for excitation of $S^{4+}$ $3s^2\ ^1S \rightarrow 3s3p\ ^1P$ transition by electron impact as a function of center-of-mass energy. Solid circles are the present absolute results with error bars representing the 90% confidence level of relative uncertainties, with the exception of the point at 16.15 eV where the outer error bar represents the total expanded uncertainty. The open squares are the present relative measurements that have been normalized to the absolute measurements. The curves are convolutions of theories with a 0.17 eV FWHM Gaussian: solid curve, eight-state CCR results of Ref. [25]; dashed curve, 31-state CCR results of Ref. [26]; dot-dashed curve, 14-state CCR results of Ref. [27]. Above 16.3 eV the results of Refs. [26,27] are indistinguishable.

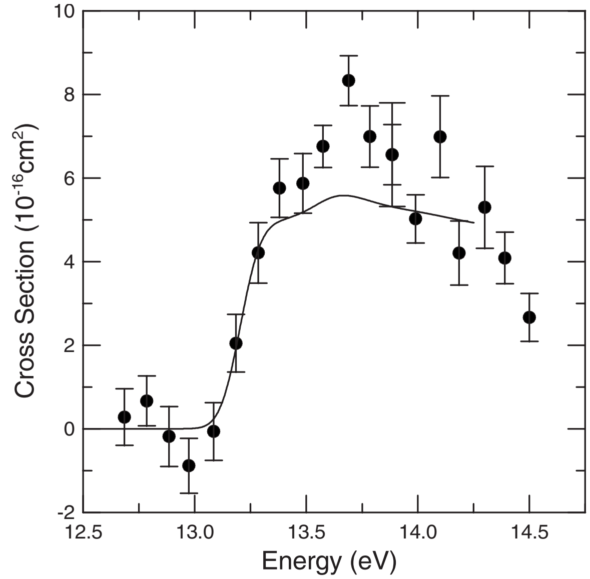


FIG. 4. Absolute cross sections for excitation of $S^{5+}$ $3s\ ^2S \rightarrow 3p\ ^2P$ transition by electron impact as a function of center-of-mass energy. Solid circles are present results with error bars representing a 90% confidence level of relative uncertainties, with the exception of the point at 13.89 eV where the outer error bar represents the total expanded uncertainty. The solid curve is a convolution of five-state CCR results of Ref. [28] with a 0.17 eV FWHM Gaussian representing the experimental energy resolution.

angle in the c.m. system may be moving backward in the laboratory frame [9]. These electrons do not reach the PSD. For the highest energies used in the present experiment, backscattering could contribute to signal loss. It is also possible for scattered electrons with large gyroradii in the solenoidal magnetic field to be blocked by the demerger apertures designed to block large-angle elastic scattering. If scattered electrons have a very low forward velocity and enter the demerger below the ground plane, so that the net potential applied by the demerger is retarding, they may be reflected by the demerger field and miss the detector. Scattered electrons may also miss the PSD on the Faraday cup side if, in order to keep the background manageable, the demerger voltage is not high enough; this is a particular concern for forward-scattered electrons. All of these losses were calculated using trajectory simulations employing the SIMION [24] code and used to correct the measured cross sections for $S^{4+}$, with corrections varying from ±1.0% at 16.35 eV to ±20% at 16.75 eV. No corrections were necessary for energies less than 16.35 eV. For the $S^{5+}$ data, the corrections varied from ±3.4% at 13.55 eV to ±21% at 14.50 eV, while no corrections were needed for energies less than 13.55 eV.

### E. Uncertainties

The relative uncertainties of the measurements are a consequence of the statistical precision of the cross-section measurements, form-factor variations between individual points, and corrections predicted by the trajectory modeling. The relative uncertainties given for the cross sections represent a 90% confidence level for statistical precision. The total expanded uncertainties of both sets of data also include the following systematic contributions, given at a level equivalent to 90% confidence for statistics: spatially delimiting the signal on the PSD (±5%), detector efficiency (±4%), absolute form factors (±12%), and electron and ion currents (±1% and ±4%, respectively). For the $S^{4+}$ measurements, additional systematic uncertainties of metastable fraction (±6%), ion beam purity (±2%), and subtraction of spurious below-threshold signal (±9%) are also included. For the $S^{5+}$ measurements, contributions of ion beam purity (±1%) and subtraction of spurious below-threshold signal (±5%) are included. Added in quadrature, these contribute about ±18% to the total expanded uncertainties for the $S^{4+}$ measurements and ±15% for the $S^{5+}$ measurements. Systematic uncertainties associated with measurement of the electron and ion velocities and with the dead time corrections are negligible.

## III. RESULTS

### A. $S^{4+}$

The measured electron-impact excitation cross sections for the $3s^2\ ^1S \rightarrow 3s3p\ ^1P$ transition in $S^{4+}$ are shown as solid symbols in Fig. 3. The error bars represent relative uncertainties at a 90% confidence level. Also shown for the data point at 16.15 eV is the total expanded uncertainty of the measurement, indicated by the outer error bars on that point. The open symbols in Fig. 3 represent relative cross-section measurements made with an ion beam contamination of $^{16}O^{2+}$ that have been normalized to the absolute measurements made with no oxygen contamination. Three calculations convoluted with a 0.17 eV Gaussian energy distribution are also shown in Fig. 3: the upper solid curve represents the eight-state close-coupling predictions of Dufton and Kingston [25], the dashed curve represents the 31-state close-coupling predictions of Kai *et al.* [26], and the dot-dashed curve represents the 14-state close-coupling calculations of Hudson and Bell. [27]. Although the three theories generally agree with the magnitude of the experimental cross sections within the total expanded uncertainty, the more rapid decrease of the experimental data at energies above the peak value at 16.0 eV suggest a resonance contribution just above threshold. This feature, evident in both the absolute and relative experimental data, is not predicted by the eight-state CCR calculations. However, the 14-state and 31-state calculations do predict a resonance in this region, but the calculations appear to underestimate its contribution to the excitation cross section.

### B. $S^{5+}$

The measured electron-impact excitation cross sections for the $3s\,^2S \rightarrow 3p\,^2P$ transition in $S^{5+}$ are shown as solid symbols in Fig. 4. The error bars represent relative uncertainties at a 90% confidence level. Also shown for the data point at 13.89 eV is the total expanded uncertainty of the measurement, indicated by the outer error bars on that point. The solid curve in Fig. 4 represents the five-state CCR calculations of Dufton and Kingston [28] convoluted with a 0.17 eV Gaussian energy distribution. The CCR predictions are in reasonable agreement with the experimental data concerning the overall magnitude of the cross section. However, the energy dependence of the experimental cross section suggests stronger contributions from dielectronic resonances than are predicted by theory, particularly near 13.7 eV.

## IV. CONCLUSIONS

In summary, absolute cross sections for electron-impact excitation of the $3s^2\,^1S \rightarrow 3s3p\,^1P$ transition in $S^{4+}$ and the $3s\,^2S \rightarrow 3p\,^2P$ transition in $S^{5+}$ have been measured using the MEIBEL technique. As was noted previously for other ions of the Na-like and Mg-like sequences, close-coupling methods are fairly accurate in predicting direct contributions to excitation for dipole-allowed transitions. However, when dielectronic resonances make significant contributions to these transitions in the near-threshold region, as they do for the $S^{4+}$ and $S^{5+}$ excitations presented here, theoretical predictions of these resonances are not nearly as accurate. This was also noted in measurements of dipole-allowed transitions for Mg-like $Si^{2+}$ and $Cl^{5+}$ ions [8,10]. The near-threshold resonance structure of the first allowed transition in Na-like $Cl^{6+}$ was reproduced well by close-coupling predictions [8]. Since the accuracy of theoretical predictions for near-threshold dielectronic resonance contributions to electron-impact excitation varies system by system, continued experimental investigations are essential to provide further guidance to the theoretical efforts.

## ACKNOWLEDGMENTS

The authors wish to thank K. A. Berrington for providing collision strengths for $S^{5+}$ based on the calculations of Dufton and Kingston. This work was supported in part by the Office of Fusion Energy Sciences and the Office of Basic Energy Sciences of the U.S. Department of Energy under Contract No. DE-AC05-00OR22725 with UT-Battelle, LLC, and by the Office of Fusion Energy Sciences of the U.S. Department of Energy under Contract No. DE-A102-95ER54293 with the National Institute of Standards and Technology. Y.S.C. was supported by the Korean Science and Engineering Foundation Grant No. R01-2001-000-00020-0.

[1] D. R. Flower and H. Nussbaumer, Astron. Astrophys. **42**, 265 (1975).
[2] F. P. Keenan, in *UV and X-Ray Spectroscopy of Laboratory and Astrophysical Plasmas*, edited by E. H. Silver and S. M. Kahn (Cambridge University Press, Cambridge, U.K., 1993), p. 44.
[3] S. O. Kastner and H. E. Mason, Astron. Astrophys. **67**, 119 (1978).
[4] D. Stutman, M. Finkenthal, H. W. Moos, K. B. Fournier, R. Kaita, D. Johnson, and L. Roquemore, Rev. Sci. Instrum. **74**, 1982 (2003).
[5] S. J. Smith, A. Chutjian, J. Mitroy, S. S. Tayal, R. J. W. Henry, K.-F. Man, R. J. Mawhorter, and I. D. Williams, Phys. Rev. A **48**, 292 (1993).
[6] M. E. Bannister, H. F. Krause, N. Djurić, D. B. Popović, G. H. Dunn, Y.-S. Chung, and A. C. H. Smith, Phys. Rev. A **66**, 032707 (2002).
[7] E. K. Wåhlin, J. S. Thompson, G. H. Dunn, R. A. Phaneuf, D. C. Gregory, and A. C. H. Smith, Phys. Rev. Lett. **66**, 157 (1991).
[8] N. Djurić, M. E. Bannister, A. M. Derkatch, D. C. Griffin, H. F. Krause, D. B. Popović, A. C. H. Smith, B. Wallbank, and G. H. Dunn, Phys. Rev. A **65**, 052711 (2002).
[9] X. Q. Guo, E. W. Bell, J. S. Thompson, G. H. Dunn, M. E. Bannister, R. A. Phaneuf, and A. C. H. Smith, Phys. Rev. A **47**, R9 (1993).
[10] B. Wallbank, N. Djurić, O. Woitke, S. Zhou, G. H. Dunn, A. C. H. Smith, and M. E. Bannister, Phys. Rev. A **56**, 3714 (1997).
[11] Y.-S. Chung, N. Djurić, B. Wallbank, G. H. Dunn, M. E. Bannister, and A. C. H. Smith, Phys. Rev. A **55**, 2044 (1997).
[12] P. A. Delamere, A. J. Steffl, and F. Bagenal, J. Geophys. Res. **109**, A10216 (2004).
[13] P. R. Young, A. K. Dupree, B. R. Espey, S. J. Kenyon, and T. B. Ake, Astrophys. J. **618**, 891 (2005).
[14] F. W. Meyer, in *Trapping Highly Charged Ions: Fundamentals and Applications*, edited by J. Gillaspy (Nova Science Publishers, Huntington, NY, 2001), p. 117.
[15] E. W. Bell, X. Q. Guo, J. L. Forand, K. Rinn, D. R. Swenson, J. S. Thompson, G. H. Dunn, M. E. Bannister, D. C. Gregory, R. A. Phaneuf, A. C. H. Smith, A. Müller, C. A. Timmer, E. K.

Wåhlin, B. D. DePaola, and D. S. Belić, Phys. Rev. A **49**, 4585 (1994).
[16] J. L. Forand, C. A. Timmer, E. K. Wåhlin, B. D. DePaola, G. H. Dunn, D. Swenson, and K. Rinn, Rev. Sci. Instrum. **61**, 3372 (1990).
[17] CIDTEC model CID 2250D solid state video camera. This information is provided for technical completeness and not as a product or company endorsement.
[18] D. C. Gregory, F. W. Meyer, A. Müller, and P. Defrance, Phys. Rev. A **34**, 3657 (1986).
[19] M. E. Bannister, Phys. Rev. A **54**, 1435 (1996).
[20] W. Lotz, Z. Phys. **261**, 241 (1968).
[21] D. H. Crandall, R. A. Phaneuf, R. A. Falk, D. S. Belić, and G. H. Dunn, Phys. Rev. A **25**, 143 (1982).
[22] J. W. G. Thomason and B. Peart, J. Phys. B **31**, L201 (1998).
[23] Y. Zhang, C. B. Reddy, R. S. Smith, D. E. Golden, D. W. Mueller, and D. C. Gregory, Phys. Rev. A **45**, 2929 (1992).
[24] D. A. Dahl, Idaho National Engineering Laboratory Report No. INEL-95/0403, 1995 (unpublished).
[25] P. L. Dufton and A. E. Kingston, J. Phys. B **17**, 3321 (1984).
[26] T. Kai, R. Srivastava, and S. Nakazaki, Phys. Rev. A **70**, 062705 (2004).
[27] C. E. Hudson and K. L. Bell, Astron. Astrophys. **452**, 1113 (2006).
[28] P. L. Dufton and A. E. Kingston, J. Phys. B **20**, 3899 (1987); K. A. Berrington (private communication).